9th International IEEE EMBS Conference on Neural Engineering
San Francisco, CA, USA, March 20 - 23 , 2019

Towards a Distributed, Chronically-Implantable Neural Interface

Nur Ahmadi*, Matthew L. Cavuto*, Peilong Feng*, Lieuwe B. Leene* *Member, IEEE,* Michal Maslik*, Federico Mazza*, Oscar Savolainen*, Katarzyna M. Szostak*, Christos-Savvas Bouganis *Senior Member, IEEE,* Jinendra Ekanayake, Andrew Jackson, Timothy G. Constandinou *Senior Member, IEEE.*

***Abstract*— We present a platform technology encompassing a family of innovations that together aim to tackle key challenges with existing implantable brain machine interfaces. The ENGINI (Empowering Next Generation Implantable Neural Interfaces) platform utilizes a 3-tier network (external processor, cranial transponder, intracortical probes) to inductively couple power to, and communicate data from, a distributed array of freely-floating mm-scale probes. Novel features integrated into each probe include: (1) an array of niobium microwires for observing local field potentials (LFPs) along the cortical column; (2) ultra-low power instrumentation for signal acquisition and data reduction; (3) an autonomous, self-calibrating wireless transceiver for receiving power and transmitting data; and (4) a hermetically-sealed micropackage suitable for chronic use. We are additionally engineering a surgical tool, to facilitate manual and robot-assisted insertion, within a streamlined neurosurgical workflow. Ongoing work is focused on system integration and preclinical testing.**

I. Introduction

Brain Machine Interfaces (BMIs) have a genuine opportunity to effect a transformative impact on both medical [1], [2] and non-medical [3] applications. More specifically, clinical translation can lead to the restoration of movement and communication in patient populations with tetraplegia, amylotrophic lateral sclerosis, locked-in-syndrome, and speech disturbances. Current translational efforts utilize implantable medical devices (IMDs), e.g. Medtronic PC+S [1], experimental neuroscience tools, e.g. Blackrock Neuroport [2], or engineer new devices leveraged on IMDs [4], [5].

A. Key Challenges

The major technical challenges with state-of-the-art BMI technology are chronic reliability (device longevity, recording stability, calibration/training) and scalability (extending number of recording and/or stimulation sites). In tackling these, wireless capability is crucial, but brings on its own set of challenges (wireless transfer efficiency, data throughput).

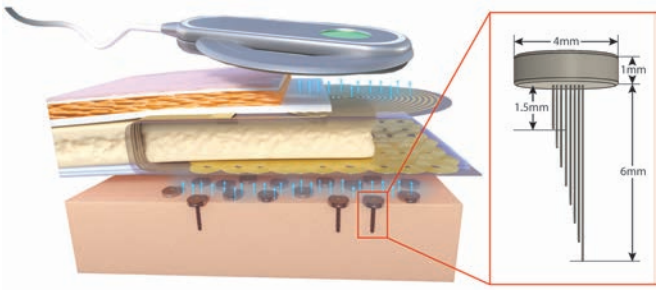

Fig. 1. ENGINI platform concept showing 3-tier link for wireless power/data transfer and single probe detail with approximate dimensions.

Furthermore, due to tight inter-dependencies between various aspects (e.g. electrodes, electronics, decoding, wireless, fabrication, packaging, surgery) a holistic approach is not only desirable but essential.

B. Next Generation Neural Interfaces

An emergent trend has been to achieve scalability by employing a distributed organization of multiple (10s to 1000s), miniature (mm or sub-mm scale) devices that are completely wireless and operate independently of one another. Wireless power transfer is achieved either by electromagnetic or ultrasonic transmission, with data encoded in the carrier (downlink) and through backscatter (uplink). Current efforts include: neural dust, using ultrasonic transduction [6]; neurograins, using electromagnetic midfield @2.6 GHz (2-coil link) [7]; using electromagnetic near-field @1 GHz (3-coil link with TDMA scheme) [8]; FF-WINeR (free-floating wireless implantable neural recording), using electromagnetic near-field @131 MHz (3-coil link with resonator) [9]; and ENIAC (encapsulated neural interfacing acquisition chip), using electromagnetic near-field @144 MHz (2-coil link) [10].

This paper presents our progress to date towards the ENGINI platform – a distributed, chronically-implantable neural interface. The remainder of the paper is organized as follows: Section I introduces the key challenges and new research directions within the community; Section II presents the specifics of our approach; Section III details the system implementation; Section IV presents results and progress to date; and Section V concludes the paper.

II. Our Approach

The ENGINI platform [11] utilizes a 3-tier network to realize a distributed architecture based on three components:

*N. Ahmadi, M.L. Cavuto, P. Feng, L. Leene, M. Maslik, F. Mazza, O. Savolainen, K.M. Szostak contributed equally to this work.

This work was supported by the UK Engineering and Physical Sciences Research Council (EPSRC) grant EP/M020975/1. Additionally, Nur Ahmadi is supported by through a Indonesia LPDP Fund graduate scholarship, and Matthew L. Cavuto is supported through the Marshall scholarship.

N. Ahmadi, M.L. Cavuto, P. Feng, L. Leene, M. Maslik, F. Mazza, O. Savolainen, K.M. Szostak, C.-S. Bouganis and T.G. Constandinou are with the Dept. of Electrical & Electronic Eng., Imperial College London, UK.

J. Ekanayake is with the Wellcome/EPSRC Centre for Interventional and Surgical Sciences, National Hospital for Neurology/Neurosurgery (Queen Square) and UCL Institute of Cognitive Neuroscience, London, UK.

A. Jackson is with the Institute of Neuroscience, Newcastle University. (Corresponding author email: t.constandinou@imperial.ac.uk)

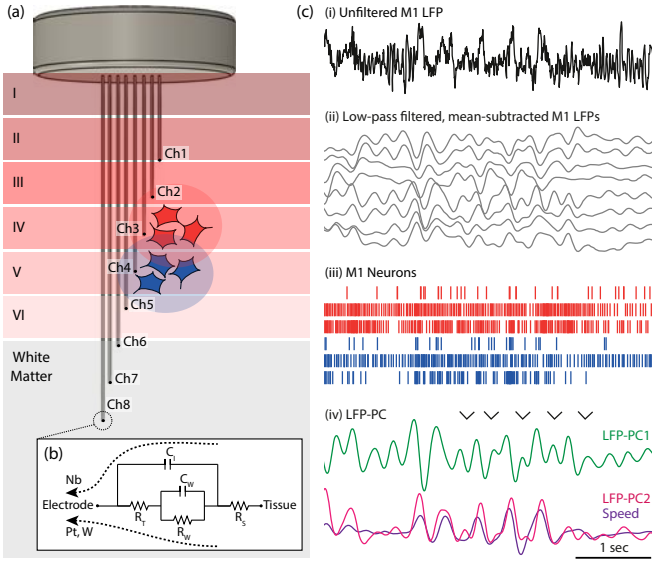

Fig. 2. (a) ENGINI probe positioned in cortex; (b) equivalent circuit of the electrode-tissue interface; (c) illustrative example of LFP recordings using microwire electrodes in M1, showing: (i) unfiltered, surface-referenced LFP from a representative electrode in M1 during task performance; (ii) low-pass-filtered, mean-subtracted LFP from 8 electrodes in the M1 array (not shown in order); (iii) spike rasters for six M1 neurons; (iv) first two principal components (LFP-PCs) calculated from low-pass filtered, mean-subtracted M1 LFPs with speed profile (isometric wrist-torque task – time derivative of radial position from origin) overlaid on LFP-PC2. Data adapted from [14].

(1) multiple mm-scale sub-dural implants for intracortical recording; (2) customized cranioplasty with embedded transponder; (3) external head-based 'processor' with battery (Fig. 1). The underlying justification for this 3-tier approach is to improve the overall wireless power transfer efficiency by more than an order of magnitude (cf. 2-coil mm-scale link [12]). This is accomplished by partitioning the link into a cm-scale transcutaneous link (similar to those used in cochlear implants), and multiple mm-scale transdural links. Additionally, by utilizing overlapping (and redundant) mm-scale coils on the subcranial primary, good uniformity in power distribution can be achieved allowing for the probes to be positioned with freedom [13]. Importantly, our approach allows the dura matter to be closed after implantation, essential for containment of cerebrospinal fluid (CSF) and reducing the risk of infection.

III. System Implementation

A. Electrodes and Neural Recording Target

To cater for maximal chronic stability of recordings, each probe uses 8 microwire electrodes to observe field potentials (LFPs) at different depths along the cortical column. While there is only a limited amount of research on the longevity of commonly used electrode types (e.g. Michigan probes, Utah arrays), there is evidence [15] to suggest that wire microelectrodes can remain functional over long periods of time. To the best knowledge of the authors, the reported uninterrupted extracellular action potential (EAP) recording of 5 years [15] is the longest achieved to date.

The achieved stability is furthermore improved by limiting the recording to LFPs [16], [17]. Chronic implantation causes growth of scar tissue due to a foreign body response, leading to spatial and temporary averaging of the sensed signals effectively leading to the formation of a low-pass filter surrounding the electrode [18]. This results in the high frequency portions of neural signals such as EAPs becoming inaccessible over time [19]. It has however been shown that low-frequency signals such as LFPs remain present for significantly longer periods [16], [20].

Since most previous neural interfaces have been designed to record EAPs, not much prior research has been done to assess suitability of various recording materials for LFP recordings. The commonly used platinum and tungsten are preferred for their chemical stability and biological compatibility in addition to favourable mechanical properties in the case of tungsten. Recording of low frequency signals are vulnerable to the resistive properties of the electrodes which are governed by diffusion. EAP recordings on the other hand, are mostly conveyed by the double-layer capacitance of the electrode-electrolyte interface leading to smaller noise content. Using a material with small diffusion currents is therefore critical to ensure capacitive conduction at as low a frequency as possible (equivalent circuit shown in Fig 2b).

Niobium is a material of a typically small diffusion current density which, in addition to its chemical stability and biological inertness, makes it suitable for use as an electrode material, achieving superior noise performance in the LFP band [21].

B. Data Minimization and Decoding Strategy

The microwire electrodes have been designed to have lengths that vary between 1.5 mm and 6.0 mm (Fig. 1), corresponding approximately to cortical layers III to VI (allowing 0.5 mm for the insertion plate – required for implantation). Each probe employs adaptive referencing to generate a set multi-channel LFP signals. These locally-referenced (differential) recordings have the effect of increasing the spatial 'focus' of the LFPs by rejecting common-mode noise from neural activity originating from further afield. This set of signals is then sorted in order of observable information content across the cortical layer of interest. An unsupervised, adaptive selection is then performed locally (in ultra-low power) to reduce the amount of data sent to the external processor (i.e. output bandwidth per probe).

The external processor then extracts the informative features from the differential LFPs. These features can be extracted from the time domain (e.g. local motor potential (LMP) [20], [22], [23]) and/or the frequency domain (e.g. power in the delta or high-gamma band [20], [23], [24]). This enables the capture of a behaviourally significant neural information [25]. The next step is to use these features for inferring the underlying spike dynamics (i.e. single-unit firing rate) [14], [16] or decoding directly the underlying behaviour [23], [26]. The former is useful for neurofeedback-based BMIs in which the participant learns to modulate their neuronal firing rate through operant reinforcement linked to implicit or explicit strategies [27]. The latter is commonly applied in biomimetic-based BMIs in which the decoder

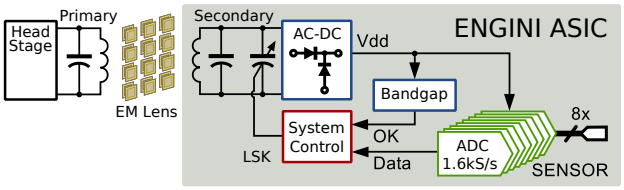

Fig. 3. Block diagram of the ENGINI recording System-on-Chip (SoC).

adapts to changes in the subject's neural activity through a calibration process.

Given that the distributed architecture can observe large scale activity through many probes, along with the non-linear and non-stationary nature of the neural signals, a commonly used linear decoder may not be optimal. Therefore, we employ deep-learning techniques that have shown state-of-the-art performance in a variety of other data analysis applications. This deep-learning based decoder will be optimized and deployed in a small, portable, and relatively low-power platform (FPGA or ASIC) for real-time application.

C. Electronic and Wireless Architecture

Each probe contains a fully integrated wireless recording system that is capable of power management, signal amplification, and data telemetry. A micro-fabricated receiving coil [12], is incorporated inside the probe micro-package that inductively harvests near-field wireless power around the 433 MHz ISM (industrial, scientific and medical) radio band. This construction relies on a passive intermediate transceiver that focuses the external power source and boosts the overall power transmission efficiency to provide uniform power distribution [13]. While the resonator and external coil can be anchored to the skull (or embedded within a customized cranioplasty), the probe is able move freely to avoid scarring as the brain experiences a variety of micro-motions.

The power regulation of the micro-system is performed autonomously in a manner that enables multiple devices to be distributed in various regions of the cortex using the same transmitter and accommodating the varying levels of electromagnetic field strength. A block diagram for one such probe is shown in Fig. 3 where we see the head-stage coupling to the ENGINI recording SoC inductively. The control block shown here digitally tunes the impedance of the resonant tank and thereby adjusts how much power is loaded from the external transmitter until the desired supply voltage is reached. This impedance is also modulated at preset frequencies to back-scatter recorded data with a unique probe identification.

The sensor itself uses multiple oversampling data converters to directly digitize the electrode recordings with high power efficiency. The modulator topology is based on a buffered DC coupled structure that provides 12 bits of dynamic range and high input impedance [28]. The first prototype amplifies signals in the 0.1–825 Hz band, has a 1.8 μV_{rms} noise figure, and can reject $> \pm 100$ mV of electrode off-set on each electrode.

TABLE I
ENGINI SENSOR SYSTEM CHARACTERISTICS

System	
Application	LFP based BMI
Supply-V	1.5 V
Total-P	92 μW
Core-A	2.1 mm^2
# Rec. Channels	8
Instrumentation	
Power/Ch	3.4 μW
Oversampling Ratio	64
Bandwidth	0.1–825 Hz
Dynamic Range	66 dB
Noise Figure	1.8 μV_{rms}
Wireless	
Modulation	LSK
Carrier Band	433 MHz
Data Rate	205 kbps
Coil - Type	Electroplated Au (25 μm) film
Coil - Size	3.5×3.5 mm^2
Coil - Inductance	5.43 nH

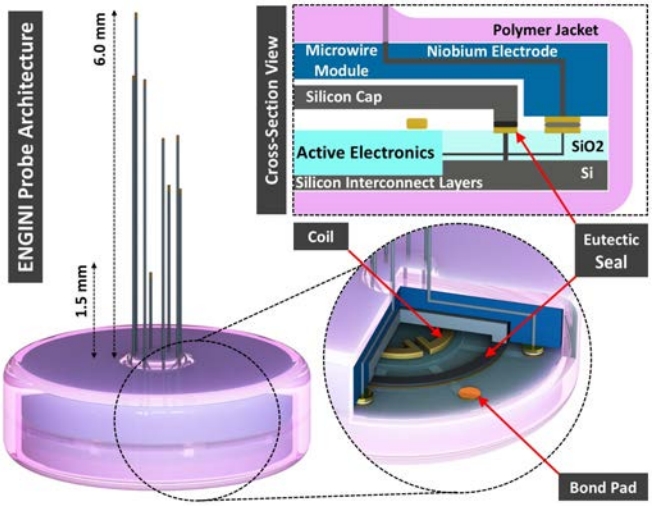

Fig. 4. ENGINI probe construction and packaging concept, combining two sub-systems: (1) hermetically-packaged microelectronic module; (2) polymer-encapsulated microwire array. Illustration not to scale.

D. Probe Construction, Packaging and Encapsulation

The ENGINI probe is constructed using standard microsystems materials and microfabrication technologies. This allows for the miniaturization of system components, parallel manufacturing and easier integration with the electronics. All materials used are biocompatible, and chosen methods ensure compatibility with CMOS – within an acceptable process temperature range. The overall structure of the probe consists of two independently-developed modules that are interconnected: (1) the micropackaged active silicon head; and (2) passive interposer that houses the microwire electrode array (Fig. 4).

The head module is comprised of two mm-sized, rounded silicon substrates joined together by a continuous seal of gold eutectic, which is robust and acts as a barrier against

moisture ingress [29]. The choice of low-temperature gold-tin eutectic as the sealant ensures compatibility with CMOS, long-term reliability and resistance to corrosion [30]. The joint is located around the edge between the substrates and as a consequence of being less than 100 μm in width, it does not significantly impact the size of the overall probe. The two substrates consist of: (1) the CMOS chip, containing the active electronics (ENGINI recording SoC), receiver coil and planar contacts buried under the layer of insulation for interconnection to the microwire module; and (2) a silicon cap, deep-etched to form the inert gas-filled cavity.

The microwire electrode array is moulded into a passive interposer structure that provides good mechanical stability and freedom in distributing the interconnections. The entire system is assembled by connecting the two modules (connections on corresponding planar surfaces) using solder (or thermocompression) bonding. An outer soft polymer jacket additionally encapsulates the assembled system and promotes tissue integration.

E. Surgical Method and Implantation Mechanism

Clinical translation will be accomplished through a stepwise procedure in line with standardized neurosurgical principles, while incorporating some novelties to reflect the unique nature of this neural interface. Following a craniotomy over the target region, a dural opening will be made to expose the cortex. With the help of a custom insertion device and accompanying anti-buckling probe architecture, which prevents buckling/bending of the delicate microwires, the required number of probes will be inserted. The dura will then be closed in a water-tight fashion over the probes, and the removed bone-flap will be replaced by a customized cranioplasty with embedded transponder.

The microwire electrodes of each probe are thin and flexible enough to help mitigate the evoked foreign body response caused by insertion and post-operative cortical micromotion [31]. Unfortunately, their flexibility also results in an increased likelihood of insertion failure, buckling, and electrode spreading. A custom insertion device has therefore been developed to address these issues, comprising a sliding anti-buckling plate and accompanying syringe applicator (Fig. 5). As the device piston is depressed, electrodes slide through the anti-buckling plate, which maintains electrode orthogonality to the cortex, bracing any deflection or bending. Once inserted to depth, the plate bonds to the probe body and the entire probe is ejected from the device.

This insertion method was selected for its ability to maintain low insertion forces, when compared to alternative methods of inserting flexible electrodes (e.g. insertion shuttles or bio-dissolvable coatings) [32]. Furthermore, ease of adoption for both manual and automated insertion ensures that the method and accompanying device is suitable in both academic and clinical settings.

IV. Preliminary Results and Ongoing Work

Several of the core methods and system components have been developed, prototyped and functionally tested, including the following: (1) mm-scale ASIC (chip); (2) microfabricated coils; (3) inductive link; (4) microwire array; (5) surgical insertion tool; (6) wafer-scale eutectic bonding (hermetic micropackaging); (7) feature extraction and decoding methods.

A. Integrated Circuit

A first generation ASIC was designed and fabricated in a commercially-available 0.35 μm CMOS technology provided by AMS AG. This initial prototype was constructed to validate our chip-scale approach, implying that a significant amount of silicon area is unused to make room for the receiving coil and seal-ring. Fig. 6 shows how the main electronic components come together before being packaged and integrated with probe shank. Initial measured results for the front-end instrumentation are shown in Fig. 7. Here we demonstrate that each probe is capable of acquiring signals with 11 bits of resolution. In this system the electromagnetic interference due to the wireless power system is mitigated through the use of continuous-time modulator topology and by minimizing the active core size.

B. Wireless Microsystem

Preliminary measurements illustrating how the operating frequency is selected for the ENGINI wireless power transfer network is shown in Fig. 8. This shows the resonant frequency of the current designed mm-scale ASIC to demonstrate that the implantable receiver can operate at the optimal frequency. As the size of the implanted devices is reduced from centimeter to millimeter, the operating frequency of the wireless power transfer system has increased from 10s of MHz to 100s of MHz. The optimal operating frequency of ENGINI wireless power transmission system is 433 MHz, which is determined by the maximum amount of power delivered to load (PDL) within the specific absorption rate (SAR) limits, while also complying with the closest ISM band. The active CMOS chip is integrated with a microfabricated Au coil (Fig. 8b), and the resonant frequency of

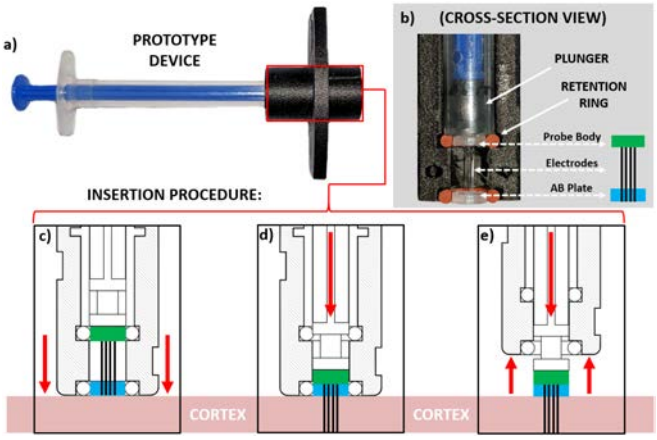

Fig. 5. a) Fully assembled insertion device; b) cross-section view of 3D printed tip showing loaded probe and respective components; c) loaded insertion device gently contacts the cortical surface; d) probe body driven downward and microwire electrodes inserted into the cortex; and e) probe ejected and device retracted.

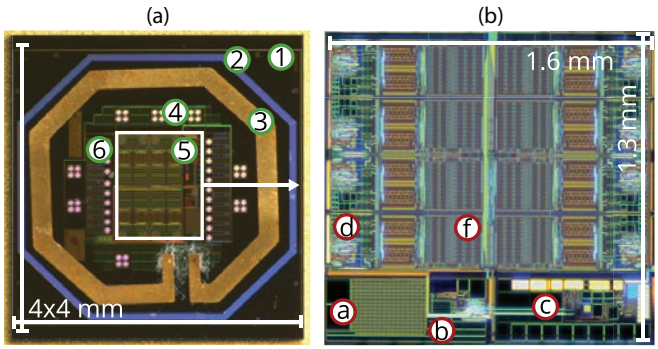

Fig. 6. Micro-photograph of the ENGINI ASIC (left) and a close-up of the electronic sub-system (right) fabricated using a C35 (0.35μm) 2P4M CMOS AMS technology. The chip is labelled as follows: ① silicon substrate, ② hermetic seal ring, ③ gold plated RF Coil, ④ Pads for feedthroughs, ⑤ active electronics, ⑥ pads for external test, ⓐ tuning capacitor, ⓑ system controller, ⓒ bandgap reference, ⓓ $\Delta\Sigma$ ADC, ⓕ CIC decimation filter.

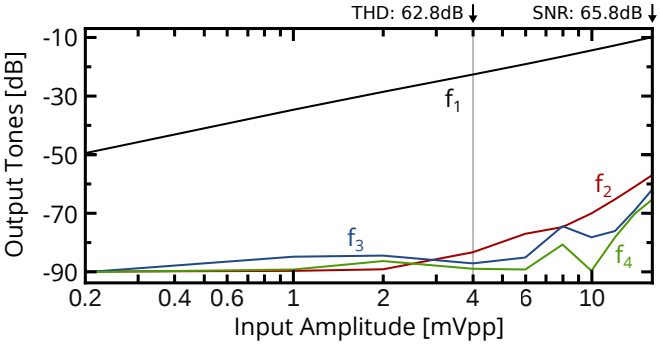

Fig. 7. Measured output harmonics with respect to the fully output range using a differential 200 Hz input sinusoid. This demonstrates a maximum SNR of 66 dB and a maximum THD of 63 dB can be achieved.

this implantable micro-system is demonstrated by measuring the reflection coefficient of this CMOS-compatible LC tank.

C. Probe Construction

As described previously (Section III-D), the probe is constructed by assembling two sub-components: (1) the probe head; and (2) the microwire array. The probe head is essentially a micropackage that houses the active CMOS electronics. One of the most critical parts here is how to form an intact hermetic seal. In order to converge on a set of near-optimal design and fabrication parameters, a series of experiments were carried out at wafer-scale (see Fig. 9a) to assess different seal frame structures [30]. Several different factors were evaluated, including the type and thickness of barrier, seed materials, deposition properties, metallurgy and geometry of the eutectic stacks. Gold-rich Au80Sn20 solder composition of thickness larger than 10 μm was selected as the best candidate for ENGINI probe's head sealing.

An early prototype of the ENGINI probe [21] is shown in Fig. 9c. This originally utilised two interposer layers (glass and silicon), with the glass interposer providing the mechanical fixation of the microwires threaded within, and the silicon interposer for achieving electrical feedthroughs and connection to the integrated circuit. This has subsequently been refined further to reduce the level of complexity in the assembly process – by alleviating the need for the two interposer layers. Mechanical stability is instead achieved by fabricating the microwire array as a separate assembly.

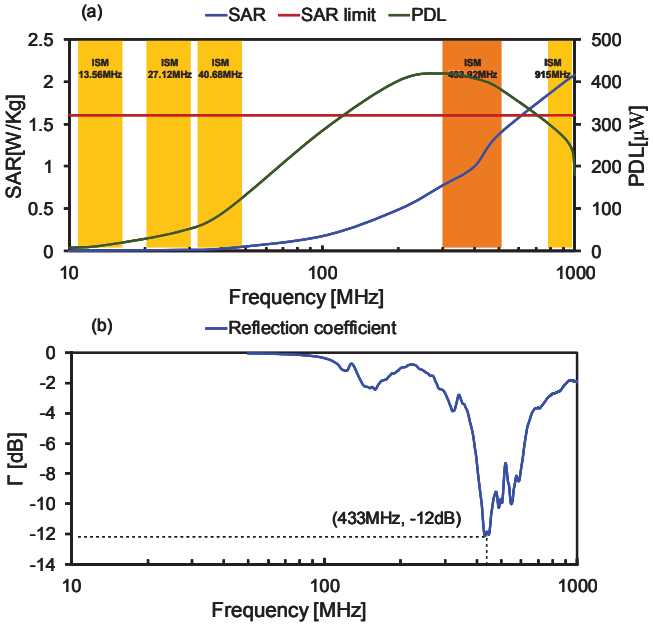

Fig. 8. (a) The optimal operating frequency of ENGINI wireless power transfer system under SAR restriction; (b) measured reflection coefficient of Voyager active chip with above-chip Au coil.

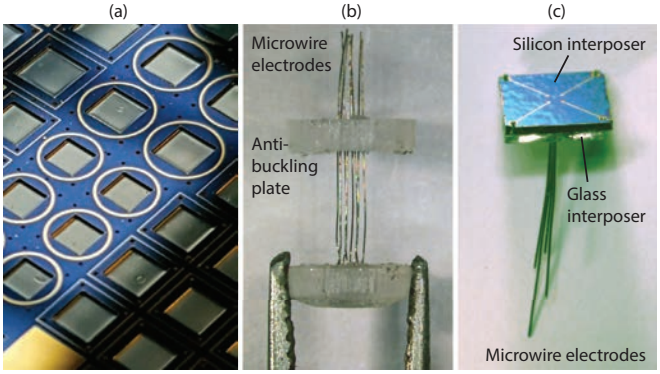

Fig. 9. Early prototypes showing: (a) micro-packaging of test probe heads (containing gas-filled cavities) with eutectic seal rings visible; (b) mock ENGINI electrode array with sliding anti-buckling plate; and (c) initial version of the probe incorporating two additional interposer layers.

Feedthroughs are formed by tunnelling connections under the seal ring using the deepest interconnect layer (e.g. metal 1 in the CMOS stack), and the electrical connection through bump/thermocompression bonding.

D. Implantation Method

The novel insertion method described previously in Section III-E was validated through a study comparing peak insertion force, electrode tip spread, and average insertion depth for three probe architectures (Fig. 10). In addition to the anti-buckling probe architecture and accompanying insertion device, "free" probes were tested, without use of the anti-buckling plate or insertion device, as well as sucrose coated probes, for which drawing lithography was used to coat the eight electrodes in a thin layer of sucrose. All three types were tested through controlled insertion, using an Instron 5543 Universal Testing System, into 0.6% by weight agarose gel. A demonstrated combination of low

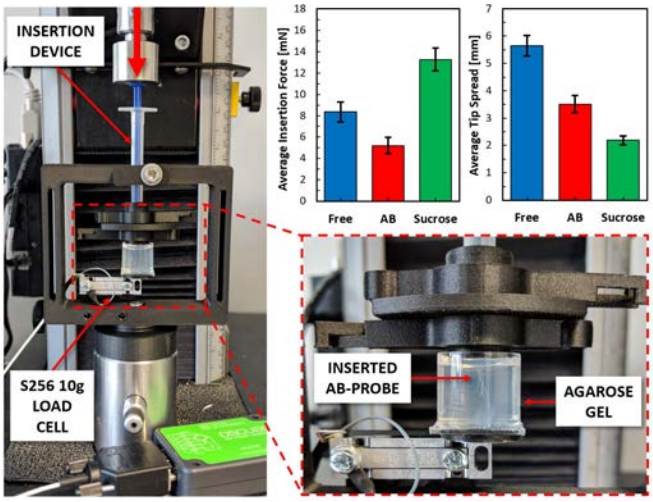

Fig. 10. Left: testing setup for novel insertion device and accompanying anti-buckling (AB) probe architecture. Right: summary results (n=10) of device and AB probe architecture compared against free and sucrose coated probes (top); and magnified view of setup post insertion trial (bottom).

insertion spread, high insertion depth, and low insertion force suggested that use of the device and anti-buckling probe architecture (Fig. 9b) was the most clinically-optimized insertion method of the three tested approaches. Further it has the potential for higher fidelity recording and decoding, while also mitigating the foreign-body response.

Ongoing work is currently focused on component refinement, system integration and *in vivo* testing.

V. Conclusion

BMIs in theory have the potential to radically change lives, but current implementations fall far short of the degree of stability and autonomy required for clinical translation. It is essential such systems work more or less 'out of the box' without requiring continual technical support or needing regular recalibration or training. A scalable solution requires a holistic system, integrating features that promote long term recording stability, patient safety, reliable surgical implantation, and diverse capability of recording and stimulation. The ENGINI system presents one such solution, leveraging a modular wireless architecture that autonomously operates to record reliable neural signals, while simultaneously maintaining a marketable and user-centric form factor.

Acknowledgment

The authors would like to thank members of the Imperial NGNI research group and project collaborators Tim Denison, Nick Donaldson, Maysam Ghovanloo and Andrew Mason.

References

[1] M. J. Vansteensel *et al.*, "Fully implanted braincomputer interface in a locked-in patient with als," *N Engl J Med*, vol. 375, no. 21, 2016.
[2] C. Pandarinath *et al.*, "High performance communication by people with paralysis using an intracortical brain-computer interface," *Elife*, vol. 6, p. e18554, 2017.
[3] S. Mitrasinovic *et al.*, "Silicon valley new focus on brain computer interface: hype or hope for new applications?" *F1000Research*, 2018.
[4] D. A. Borton *et al.*, "An implantable wireless neural interface for recording cortical circuit dynamics in moving primates," *J Neural Eng*, vol. 10, no. 2, p. 026010, 2013.
[5] C. S. Mestais *et al.*, "WIMAGINE: wireless 64-channel ecog recording implant for long term clinical applications," *IEEE Trans Neural Syst Rehabil Eng*, vol. 23, no. 1, pp. 10–21, 2015.
[6] D. Seo *et al.*, "Neural dust: An ultrasonic, low power solution for chronic brain-machine interfaces," *arXiv:1307.2196*, 2013.
[7] J. S. Ho *et al.*, "Midfield wireless powering for implantable systems," *P IEEE*, vol. 101, no. 6, pp. 1369–1378, June 2013.
[8] A. Nurmikko, "Approaches to large scale neural recording by chronic implants for mobile BCIs," in *6th Int Conf BCI*, 2018, pp. 1–2.
[9] P. Yeon *et al.*, "Fabrication and microassembly of a mm-sized floating probe for a distributed wireless neural interface," *Micromachines*, vol. 7, no. 9, p. 154, 2016.
[10] S. Ha *et al.*, "Silicon-integrated high-density electrocortical interfaces," *P IEEE*, vol. 105, no. 1, pp. 11–33, 2017.
[11] T. G. Constandinou and A. Jackson, "Implantable neural interface," 2016, WO/2017/199052.
[12] P. Feng *et al.*, "Chip-scale coils for millimeter-sized bio-implants," *IEEE Trans Biomed Circuits Syst*, no. 99, pp. 1–12, 2018.
[13] P. Feng and T. G. Constandinou, "Robust wireless power transfer to multiple mm-scale freely-positioned neural implants," in *Proc IEEE Biomed Circuits Syst Conf (BioCAS)*, 2018, pp. 1–4.
[14] T. M. Hall *et al.*, "A common structure underlies low-frequency cortical dynamics in movement, sleep, and sedation," *Neuron*, vol. 83, no. 5, pp. 1185–1199, 2014.
[15] D. A. Schwarz *et al.*, "Chronic, wireless recordings of large-scale brain activity in freely moving rhesus monkeys," *Nature Methods*, vol. 11, no. 6, p. 670, 2014.
[16] T. M. Hall *et al.*, "Real-time estimation and biofeedback of single-neuron firing rates using local field potentials," *Nature Comms*, vol. 5, p. 5462, 2014.
[17] K. M. Szostak *et al.*, "Neural interfaces for intracortical recording: Requirements, fabrication methods, and characteristics," *Front Neurosci*, vol. 11, p. 665, 2017.
[18] M. S. Fee *et al.*, "Variability of extracellular spike waveforms of cortical neurons," *J Neurophysiol*, vol. 76, no. 6, pp. 3823–3833, 1996.
[19] M. D. Linderman *et al.*, "Neural recording stability of chronic electrode arrays in freely behaving primates," in *Conf Proc IEEE Eng Med Biol Soc*, 2006, pp. 4387–4391.
[20] R. D. Flint *et al.*, "Accurate decoding of reaching movements from field potentials in the absence of spikes," *J Neural Eng*, vol. 9, no. 4, p. 046006, 2012.
[21] K. M. Szostak *et al.*, "Microwire-CMOS integration of mm-scale neural probes for chronic local field potential recording," in *Proc IEEE Biomed Circuits Syst Conf (BioCAS)*, 2017, pp. 1–4.
[22] R. D. Flint *et al.*, "Long term, stable brain machine interface performance using local field potentials and multiunit spikes," *J Neural Eng*, vol. 10, no. 5, p. 056005, 2013.
[23] S. D. Stavisky *et al.*, "A high performing brain–machine interface driven by low-frequency local field potentials alone and together with spikes," *J Neural Eng*, vol. 12, no. 3, p. 036009, 2015.
[24] J. Zhuang *et al.*, "Decoding 3-d reach and grasp kinematics from high-frequency local field potentials in primate primary motor cortex," *IEEE Trans Biomed Eng*, vol. 57, no. 7, pp. 1774–1784, 2010.
[25] M. W. Slutzky and R. D. Flint, "Physiological properties of brain-machine interface input signals," *J Neurophysiol*, vol. 118, no. 2, pp. 1329–1343, 2017.
[26] T. Milekovic *et al.*, "Stable long-term BCI-enabled comm. in ALS and locked-in syndrome using LFP signals," *J Neurophysiol*, 2018.
[27] A. Jackson and T. M. Hall, "Decoding local field potentials for neural interfaces," *IEEE Trans Neural Syst Rehab Eng*, vol. 25, no. 10, 2017.
[28] L. B. Leene *et al.*, "Autonomous SoC for neural local field potential recording in mm-scale wireless implants," in *Proc IEEE Int Symp Circ Syst (ISCAS)*, 2018, pp. 1–5.
[29] F. Mazza *et al.*, "Integrated devices for micro-package integrity monitoring in mm-scale neural implants," in *Proc IEEE Biomed Circuits Syst Conf (BioCAS)*, 2018, pp. 1–4.
[30] K. M. Szostak and T. G. Constandinou, "Hermetic packaging for implantable microsystems: effectiveness of sequentially electroplated AuSn alloy," in *Conf Proc IEEE Eng Med Biol Soc*, 2018, pp. 3849–3853.
[31] A. Stiller *et al.*, "A Meta-Analysis of Intracortical Device Stiffness and Its Correlation with Histological Outcomes," *Micromachines*, 2018.
[32] A. Weltman *et al.*, "Flexible, Penetrating Brain Probes Enabled by Advances in Polymer Microfabrication," *Micromachines*, vol. 7, no. 12, p. 180, 10 2016.